Analytical model for the open-circuit voltage and its associated resistance in organic planar heterojunction solar cells

D. Cheyns,* J. Poortmans, and P. Heremans
IMEC v.z.w., Kapeldreef 75, 3001 Leuven, Belgium
and ESAT, Katholieke Universiteit Leuven, Kasteelpark Arenberg 10, B-3001 Leuven, Belgium

C. Deibel,† S. Verlaak, B. P. Rand, and J. Genoe
IMEC v.z.w., Kapeldreef 75, 3001 Leuven, Belgium

(Received 15 January 2008; revised manuscript received 2 April 2008; published 22 April 2008)

We derive an analytical formula for the open-circuit voltage (V_{oc}) of organic planar heterojunction solar cells under standard operating conditions. We find that the type of free carrier recombination at the interface between the donor and acceptor materials controls the slope of V_{oc} vs incident light intensity. By using the same derivation, an equation for the resistance around V_{oc} is obtained. From this, we investigate two parameters in more detail and compare them to experiments. The first is the work function of the cathode metal. We show that, within our model, V_{oc} does not depend on this work function, while the cell resistance around V_{oc} is strongly dependent on it. Second, we find that the asymptotic resistance around V_{oc} is a third-order power function of the thickness of the organic layers (acceptor or donor). The model provides insights to achieve low-resistivity high open-circuit voltage organic solar cells.

DOI: 10.1103/PhysRevB.77.165332 PACS number(s): 72.20.Jv, 72.80.Le, 73.40.Lq

I. INTRODUCTION

Despite growing research efforts, the fundamental processes governing the operation of organic diodes are still poorly understood. A better understanding would guide improvements in device design and performance. One application of organic diodes is in the area of solar cells, and a key parameter that can reveal physical mechanisms underlying the diode operation is the open-circuit voltage (V_{oc}). It determines the point where the solar cell stops working as an active device. Organic solar cells consisting of a donor-acceptor bilayer have been shown to cover a broad range of open-circuit voltages[1–10] ranging from 0.25 to 2 V. The value strongly depends on the chosen material set. Several models described in literature, which are based on equivalent circuit modeling,[11] experimental work,[12] or semianalytical approaches,[13,14] indicate that the maximum open-circuit voltage of a chosen material set is limited by the difference of the highest occupied molecular orbital (HOMO) of the donor and the lowest unoccupied molecular orbital (LUMO) of the acceptor.[12,13,15,16]

The maximum power produced by a solar cell is in part determined by the voltage at the maximum power point, which is close to the open-circuit voltage. This maximum power point is parametrized by the fill factor (FF), a figure of merit indicating how close the current-voltage (I-V) characteristics under illumination are to an ideal rectangular shape. Any parasitic resistance will reduce the fill factor and thus the overall efficiency.[17,18]

In this work, we derive an analytical model for V_{oc} based on exciton dissociation at the interface between two materials. Starting from first principles, it is shown that V_{oc} is largely determined by a diffusion current of carriers away from the interface between the donor and acceptor materials. In the next step, the model is extended to calculate the resistance at V_{oc}, which plays a crucial role in determining FF. Simulations are carried out to obtain the carrier density and the electric field distribution inside the device, which control the resistance. Finally, we compare our results to experimental data in order to verify our model.

II. MODEL

A. Analytical formulas for the open-circuit voltage

The schematic energy diagram of a planar heterojunction solar cell is shown in Fig. 1. Once an exciton reaches the interface between the donor and the acceptor, it will dissociate to a bound polaron pair with a certain probability. In order to generate free polarons (i.e., a free electron in the acceptor and a free hole in the donor), the Coulombic polaron pair binding energy has to be overcome. These carriers will then be mobile in their respective transport levels within the LUMO of the acceptor (LUMO_A) and the HOMO of the donor (HOMO_D). The maximum energy, which can be extracted, is given by the difference between these two levels, $|\mathrm{HOMO}_D|-|\mathrm{LUMO}_A|$. We note that, for the purpose of this model, any dipoles between the two organic layers are included in this difference. Carriers can gain or lose energy during their transport in the layers due to the band bending of the electrostatic potential (BB_D and BB_A, as shown in Fig. 1). At the contacts, the carriers can be extracted, which leads to an additional energy loss originating from the difference of metal work function to the energy levels of the organic layers ($\Delta\phi_A$ and $\Delta\phi_D$). Again, all possible dipoles or pinning effects are included in these offsets.

If the device is working under open-circuit conditions, moving one electron and one hole from the donor-acceptor interface toward the electrodes will yield the voltage across the device. This corresponds to

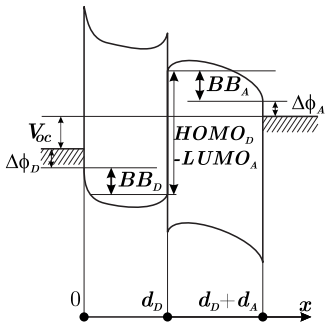

FIG. 1. Schematic energy diagram of a planar heterojunction solar cell. $|\mathrm{HOMO}_D|-|\mathrm{LUMO}_A|$ is the energy difference between the HOMO of the donor and the LUMO of the acceptor, BB_A and BB_D are the net band bendings in the electrostatic potential, and $\Delta\phi_A$ and $\Delta\phi_D$ are the energy offsets at the contact. The values of BB_A and BB_D are negative if a carrier moving from the interface to the contact loses energy and are positive if the carrier gains energy. As the acceptor layer is an electron region, and the donor layer a hole region, BB_A and BB_D ($\Delta\phi_A$ and $\Delta\phi_D$), show an opposite bending for the same sign. At the bottom, the coordinate system is drawn, with d_D and d_A as the thickness of the donor and acceptor layers, respectively.

$$V_{\mathrm{oc}} = |\mathrm{HOMO}_D| - |\mathrm{LUMO}_A| + \mathrm{BB}_D + \mathrm{BB}_A - \Delta\phi_A - \Delta\phi_D. \tag{1}$$

We will see later that the effect of the band bending will compensate for the energy loss at the contacts, making V_{oc} independent of the work function of the electrodes.

In order to calculate the band bending of a bilayer of undoped semiconductors, we apply the Poisson equation,

$$\nabla \cdot \vec{F} = \frac{q \cdot (p-n)}{\varepsilon}, \tag{2}$$

and the continuity equations of electrons and holes,

$$\frac{dp}{dt} = -\nabla \cdot (p\mu_p \vec{F} - D_p \vec{\nabla} p) + G_p - \mathrm{Rec}_p \tag{3}$$

$$\frac{dn}{dt} = -\nabla \cdot (n\mu_n \vec{F} + D_n \vec{\nabla} n) + G_n - \mathrm{Rec}_n. \tag{4}$$

Here, q is the elementary charge, ε is the absolute permittivity that we assume the same for both layers, p and n are the concentrations of holes and electrons, μ_p and μ_n are the hole and electron mobilities, D_p and D_n are the hole and electron diffusion constants, G_p and G_n are carrier generation rates, and Rec_p and Rec_n are recombination rates, respectively. If solved self-consistently, the solutions yield the electron and hole densities (n and p) as well as the electric field ($\vec{F}$) within the film. We assume the device to be in steady state (dp/dt and dn/dt are 0), the doping concentrations to be negligible compared to the free carrier concentration and the Einstein relation ($D/\mu = kT/q$, where k is the Boltzmann constant and T is the absolute temperature) to hold.

The equations will be derived for a homogeneous planar heterojunction. For symmetry reasons, we consider the one-dimensional case. The vectors can be represented by their magnitude, and the gradients and divergences resolve into simple derivatives. In the following, the derivation will be outlined for the donor layer. The results for the acceptor layer are analogous.

The band bending due to the change in electrical potential is equal to

$$\mathrm{BB}_D = \int_0^{d_D} F(x)dx, \tag{5}$$

where d_D is the thicknesses of the donor layer. We define the donor contact to be located at point $x=0$ and the donor-acceptor interface at $x=d_D$ (see the bottom of Fig. 1).

Starting from an expression for the current, the field $F(x)$ is evaluated. As the equations will be derived for the hole-conducting donor material, we neglect the electron density. By doing so, we assume a metal contact that is not injecting any electrons. Therefore, the total current in the donor layer equals the hole current,

$$j_p = q\mu_p \left(pF - \frac{kT}{q}\frac{dp}{dx} \right), \tag{6}$$

with $j_p=0$ for the case under investigation (V_{oc}). Analytical solutions for the carrier density and electric field as a function of position can be derived, as shown in Appendix A.

By using Eqs. (5) and (6) with $j_p=0$, the net band bending can be rewritten as

$$\mathrm{BB}_D = \frac{kT}{q} \ln\left(\frac{p_i}{p_c} \right). \tag{7}$$

The carrier concentration at the interface p_i will be determined by the incident light intensity, whereas the carrier concentration at the contact p_c is a function of the barrier $\Delta\phi_D$.

The result of Appendix A can be used to calculate the carrier profile inside an organic solar cell. Figure 2 shows an example of simulations carried out for a 50 nm thick layer of organic material. The carrier density at the contact p_c is fixed to three different values, and for each value, a different p_i is used. The steady-state carrier density through the layer is plotted, depending on the boundary condition.

B. Carrier concentration at the contact

The physics at the interface between a metal and an organic semiconductor remains a matter of discussion. For an overview of the current state of understanding, see reviews by Scott[19] and Arkhipov.[20] While not going into detail here, the carrier density at the interface is given by an exponential dependence on the injection barrier ($\Delta\phi_D$) and some dependence on field and temperature, depending on the model applied. The injection barrier can be calculated from the position of the HOMO or LUMO and the metal work function, taking into account any surface dipoles.[21] Additionally, the metal work function itself depends on possible oxidation or surface contaminations.[22] Therefore, the $\Delta\phi_D$ used here is an effective injection barrier, accounting for all such effects.

A general equation for the carrier density at the contact can be written as

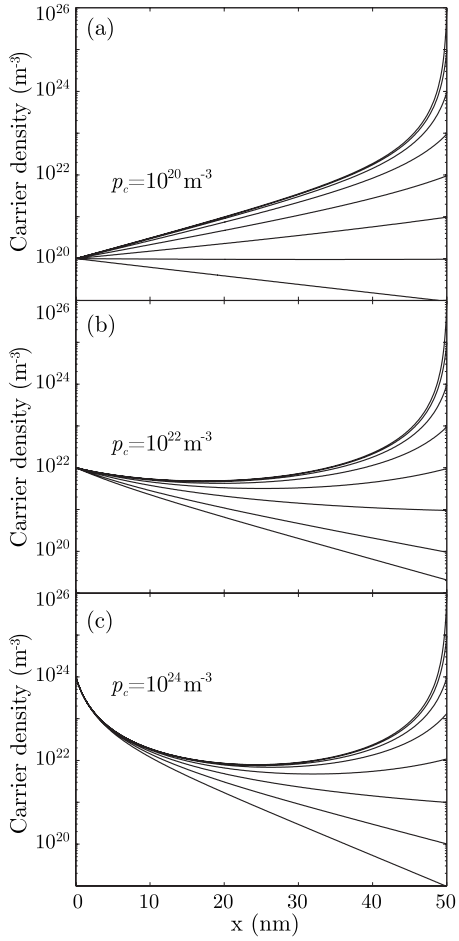

FIG. 2. Modeled carrier density versus position, where $x=0$ nm is equal to the contact and $x=50$ nm is the location of the heterojunction. The different graphs correspond to different carrier densities at the contact [(a) 10^{20}, (b) 10^{22}, and (c) 10^{24} carriers/m^3], while the different curves on each graph correspond to different carrier densities at the interface ranging from 10^{19} to 10^{26} carriers/m^3.

$$p_c = N_D f(F_c) \exp\left(-\frac{\Delta\phi_D}{kT/q}\right), \tag{8}$$

where N_D is the effective density of states of the donor and $f(F_c)$ is a function to include the effect of the electric field at the contact. An example is the Richardson–Schockley[23] equation for thermionic emission with field dependent barrier lowering,

$$p_c = N_D \exp\left(-\frac{\Delta\phi_D - \Delta_{\text{low}}(F)}{kT/q}\right), \tag{9}$$

with

$$\Delta_{\text{low}}(F) = \sqrt{\frac{q^3 F}{4\pi\varepsilon}}. \tag{10}$$

The effective reduction in the barrier is introduced to take the image charge into consideration. This effect occurs only if the field is aiding carrier injection, pointing away from the contact for electrons (acceptor layer) and pointing toward the contact for holes (donor layer). Otherwise, $\Delta_{\text{low}}(F)$ is zero.

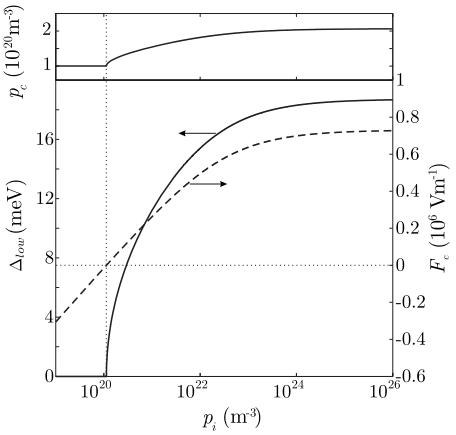

FIG. 3. Effect of field dependent barrier lowering (Δ_{low}). Simulations are carried out by using an injection barrier $\Delta\phi_D=0.42$ eV, giving a contact carrier density (p_c) of 1×20 m^{-3} without barrier lowering. The lower graph plots the field at the contact (F_c) needed to reach a certain carrier density at the interface. When a positive field is present, barrier lowering occurs and p_c increases (upper panel). Note that it only increases by a factor of 2 for an increase in p_i of 6 orders of magnitude.

By combining Eqs. (1), (7), and (9), we obtain the following expression for V_{oc}:

$$V_{\text{oc}} = |\text{HOMO}_D| - |\text{LUMO}_A| + \frac{kT}{q}\ln\left(\frac{p_i}{N_D}\right) + \frac{kT}{q}\ln\left(\frac{n_i}{N_A}\right) + \Delta_{\text{low}}(F_{c,D}) + \Delta_{\text{low}}(F_{c,A}). \tag{11}$$

The terms that determine V_{oc} are mainly HOMO_D, LUMO_A and the carrier concentration achievable at the interface. The concentration of photogenerated carriers at the interface can never exceed the density of states. As a consequence, the open-circuit voltage will be limited by the effective energy offset between the HOMO of the donor and the LUMO of the acceptor,[16] in practice, V_{oc} will always be lower. The influence of the barrier lowering by the field at the contact is expected to be less than 20 meV, as can be seen in Fig. 3.

Furthermore, it appears that V_{oc} is not dependent on the work function of the contact materials. Figure 4 plots the schematic energy diagram and the carrier profile inside the organic layers for two different contact materials, leading to two different injection barriers. The carrier density at the donor-acceptor interface is the same for both plots. When the work function of the contact material leads to a low injection barrier, the carrier profile generates a diffusion current toward the interface [Fig. 4(a)]. As the net current is zero at V_{oc}, a counteracting drift current pointing away from the interface should cancel this diffusion current. The resulting band bendings (BB_A and BB_D) are negative terms in Eq. (1). In contrast, when the chosen contact leads to a high injection barrier, the diffusion current due to the carrier profile points toward the contacts [Fig. 4(b)]. In the end, the obtained V_{oc} is the same for

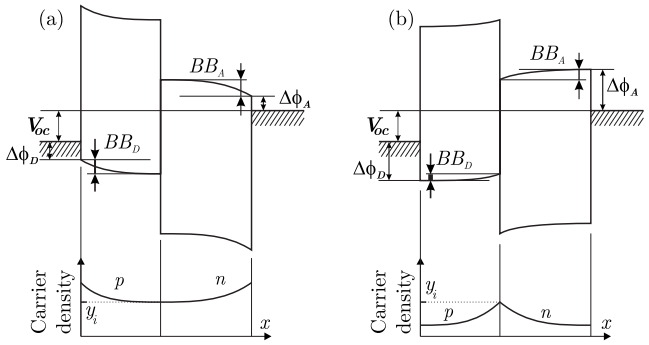

FIG. 4. Schematic energy diagrams (upper graphs) and corresponding carrier profile in the organic layers (lower graphs) when using (a) low and (b) high injection barriers at the contacts, $\Delta\phi_D$ and $\Delta\phi_A$. The same incident light intensity is used for the two situations, creating the same density of carriers at the donor-acceptor interface (y_i). The values for the band bendings, BB_A and BB_D, are negative for (a) and positive for (b). The resulting open-circuit voltage V_{oc} is the same.

both situations. The results of our analytical model are in agreement with the numerical calculations in the previous work.[13,24]

C. Carrier density at the interface

The conversion of light into free charge carriers at the interface is a three-step process:

(1) The absorbed light creates *excitons*.

(2) The excitons diffuse toward the interface where dissociation into *polaron-pairs* occurs.

(3) These polaron pairs need to further dissociate to create *free charge carriers.*

At the interface, three continuity equations are needed for the three particles involved, namely, for excitons [S, Eq. (12)], polaron pairs [X, Eq. (14)], and free carriers [holes in this example, $p_{i,s}$, Eq. (15)]. The equations for polaron pairs and free carriers are written for surface densities (particles per area), while a conversion to bulk densities can be done assuming all surface reactions take place at a monolayer from the interface. The exciton continuity equation is

$$\frac{dS}{dt} = G_S - \mathrm{Rec}_S - D_S\frac{d^2S}{dx^2}, \tag{12}$$

with a boundary condition at the interface,

$$D_S \left.\frac{dS}{dx}\right|_i = G_X. \tag{13}$$

Here, G_S is the generation of excitons due to incident light, Rec_S incorporates all possible exciton recombination mechanisms, D_S is the diffusion constant for the excitons, and G_X is the amount of dissociated excitons into polaron pairs.

For the polaron pairs, we obtain

$$\frac{dX}{dt} = G_X - k_{X,\mathrm{rec}}X - k_{\mathrm{diss}}X + \mathcal{L}n_{i,s}p_{i,s}, \tag{14}$$

where $k_{X,\mathrm{rec}}$ is the recombination rate, k_{diss} is the rate of dissociation into free carriers, and $\mathcal{L}n_{i,s}p_{i,s}$ is the creation of excitons due to Langevin-type recombination of free carriers.

The free carrier continuity equation is

$$\frac{dp_{i,s}}{dt} = k_{\mathrm{diss}}X - \mathcal{L}n_{i,s}p_{i,s} - k_{\mathrm{SRH}}\frac{n_{i,s}p_{i,s}}{n_{i,s}+p_{i,s}}. \tag{15}$$

with the last term reflecting Shockley–Read–Hall (SRH) recombination.

In order to calculate the generation of excitons [G_S in Eq. (12)], one should take into account the optical interference.[25,26] The generation has a linear dependence on the light intensity ($G_S \propto P_0$). At low to medium light intensities, the exciton recombination term Rec_S is directly proportional to the exiton density. Only at very high light intensities, recombination mechanisms such as singlet-singlet or singlet-polaron quenching will become important. As long as these multiple-particle effects can be neglected, the number of dissociated excitons will have a linear dependence on incident light intensity ($G_X = \alpha P_0$).

Polaron pairs are created from the dissociation of excitons at the heterojunction. Coulombic attractive forces prevent these particles from dissociating into free carriers. The two rates (recombination $k_{X,\mathrm{rec}}$ and dissociation k_{diss}) will determine the probability of dissociation into free carriers.[27]

The free carriers obtained in this way can return to a polaron pair with a rate constant $\mathcal{L}$, which is the Langevin recombination rate. As such, polaron pairs can be dissociated and created multiple times before the carriers are collected to the contacts.[13,28] The last recombination term in Eq. (15) reflects the recombination at the interface due to surface traps. This trap-assisted recombination process can be expressed with the SRH equation.[29–32] The recombination rate k_{SRH} takes the trap density and the capture coefficients of electrons and holes into account.

The assumption $n_{i,s} = \zeta p_{i,s}$ is made to relate the opposite charge carriers; both will have the same light dependence as they are created and recombined. Combining Eqs. (12), (14), and (15) with the continuity equation for electrons, we obtain a quadratic equation for the carrier density at the interface,

$$\mathcal{L}\zeta \cdot p_{i,s}^2 + k_{\mathrm{SRH}}\frac{\zeta}{1+\zeta}\left(1 + \frac{k_{\mathrm{diss}}}{k_{X,\mathrm{rec}}}\right)p_{i,s} - \frac{k_{\mathrm{diss}}}{k_{X,\mathrm{rec}}}\alpha P_0 = 0. \tag{16}$$

Depending on which recombination mechanism dominates at the interface, Eq. (16) can be simplified. If bimolecular Langevin-type recombination is the important limiting factor, the carrier density can be expressed as

$$p_{i,s} = \sqrt{\frac{1}{\zeta}\frac{k_{\mathrm{diss}}}{k_{X,\mathrm{rec}}\mathcal{L}}\alpha P_0}. \tag{17}$$

The solution in case of SRH recombination is

$$p_{i,s} = \frac{k_{\mathrm{diss}}}{k_{\mathrm{SRH}}}\frac{1+\zeta}{\zeta(k_{\mathrm{diss}}+k_{X,\mathrm{rec}})}\alpha P_0. \tag{18}$$

The final equation relating the V_{oc} and the incident light is obtained by combining Eqs. (11), (17), and (18). Simplified, the V_{oc} can be expressed by

$$V_{oc} = |\mathrm{HOMO}_D| - |\mathrm{LUMO}_A| + n_{voc}\frac{kT}{q}\ln\left(\frac{\kappa}{N_A N_D}\alpha P_0\right) + \Delta_{low}(F_{c,D}) + \Delta_{low}(F_{c,A}), \quad (19)$$

where n_{voc} and κ are the factors determined by the actual recombination processes for the electrons and holes at the interface.

According to Eq. (19), V_{oc} has a logarithmic dependence on light, with a slope per decade equal to $2.3n_{voc}kT/q$. If both carrier types are limited by bimolecular recombination, n_{voc} is equal to 1, while a value of 2 is obtained if SRH recombination determines the electron and hole densities. These values corresponds to a slope of 60 or 120 mV/decade. Only one slope dominates at a given light intensity, but a transition from SRH recombination at low light intensities to bimolecular recombination at high light intensities is possible, and this will be reflected in two different slopes for V_{oc} as a function of $\log(P_0)$.

The different parameters directing n_i and p_i are assumed to be electric field independent. In certain cases, this assumption can be violated,[27] and this will have a direct impact on the slope of V_{oc}. Also, the choice of metal contact can influence the electrical field at the interface, and as such, V_{oc}.

D. Resistivity around V_{oc}

The resistivity at V_{oc} is a measure for the quality of the solar cell, as it influences the FF. It can be calculated starting from Eq. (6),

$$F = \frac{kT}{q}\frac{\partial \ln(p)}{\partial x} + \frac{j}{pq\mu_p}. \quad (20)$$

By using this relationship together with Eqs. (1) and (5) (which are equations valid for any voltage applied over the contacts, not only for V_{oc}), we obtain a formula that is valid for the whole I-V curve,

$$V(j) = |\mathrm{HOMO}_D| - |\mathrm{LUMO}_A| + \frac{kT}{q}\ln\left(\frac{p_i}{N_D}\right) + \frac{kT}{q}\ln\left(\frac{n_i}{N_A}\right) + jR(j), \quad (21)$$

with $R(j)$ as an extra resistance, which gives the slope of the I-V curve for a certain current. When the bias reached is close to V_{oc}, we can assume the carrier concentration at the interface and the contact to be constant. The voltage across the device is equal to V_{oc}, with the addition of the term jR_{voc}. The resistance is given by

$$R_{voc} = \frac{1}{q}\left(\int_0^{d_D}\frac{dx}{\mu_p p} + \int_{d_D}^{d_D+d_A}\frac{dx}{\mu_n n}\right). \quad (22)$$

This integral can be solved and an analytic formula is obtained. The results are shown in Appendix B.

Equation (22) expresses the importance of reasonable mobilities for low resistance devices. However, another important parameter is the carrier concentration profile inside the organic layer. Low carrier densities, whether at the contacts, at the interface or in the bulk, will lead to high resistance, as shown by Eq. (22). By changing the metal contacts, the carrier concentration profile may drastically change, and accordingly, the resistance will change. Another important parameter is the thickness of the layer. It directly influences the resistance by both increasing the carrier transport path length and by altering the carrier concentration profile. Simulations and experiments will be carried out below to illustrate these points.

III. EXPERIMENT

In order to verify the model derived in Sec. II, we performed various experiments with organic solar cells based on copper phthalocyanine (CuPc) as the donor material and *N*,*N*′-di-tridecyl-3,4,9,10-perylene tetracarboxylic diimide (PTCDI-$C_{13}H_{27}$) as the electron acceptor. On some samples, a thin layer of bathocuproine (BCP) is added prior to metal deposition. The substrates consist of 100 nm thick indium tin oxide layer (ITO, Merck) on glass, with a sheet resistance of $<20\ \Omega/\square$. They are cleaned with soap, de-ionized water, acetone, and isopropanol. A 15 min UV-ozone treatment is carried out prior to the deposition of the organic layers. All organic molecules are purchased from Aldrich and are purified once by gradient sublimation. All layers are deposited under ultrahigh vacuum conditions (base pressure below 1×10^{-8} Torr). The layers are subsequently deposited without breaking vacuum except for mounting the shadow masks for electrode deposition inside a nitrogen atmosphere.

Illumination is with a 1000 W xenon arc lamp equipped with filters to simulate the AM1.5D spectrum (L.O.T. oriel solar simulator). The lamp is calibrated by using a bandpass filter (KG5, L.O.T. oriel[33]) and a silicon detector. The incident light power is varied with neutral density filters.

IV. RESULTS AND DISCUSSION

A. Simulation

The results of Sec. II can now be applied to calculate the carrier and electric field profiles in the different layers as a function of the incident light intensity. Initially, we choose a certain electric field at the contact F_c. Depending on the injection model, the carrier density at the contact (p_c) is calculated. From these two values, we calculate the field and carrier profile in the layer. By changing the value of F_c, a range of values for the carrier density (p_i) and field ($F_{i,D}$) at the interface is obtained. These steps are then repeated for the acceptor layer, giving a range of n_i and $F_{i,A}$ values. As the electric field should be continuous at the interface ($F_{i,D}=F_{i,A}$, if the permittivities of the materials are the same), the profiles for the different layers can be linked to each other. Finally, by using Eq. (17) or (18), the incident light required to obtain a certain n_i-p_i couple can be calculated.

Because it is difficult to correlate carrier density with incident light intensity, most of the plots used in this paper give the carrier density at the interface on the x axis, and not the incident light intensity. In all the simulations, the mobility of the organic layers is fixed to 1×10^{-7} $\mathrm{m^2/V\,s}$, while the effective density of states is kept at 1×10^{27} $\mathrm{states/m^3}$.

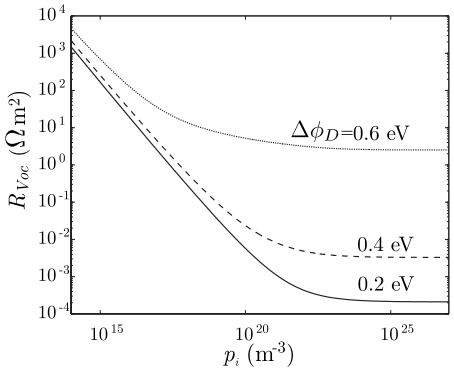

FIG. 5. Calculated resistance at V_{oc} as a function of the carrier density at the interface p_i by using different injection barriers $\Delta\phi_D$, and this for a 50 nm thick layer with a mobility of 1×10^{-7} m^2/V s.

B. Change in work function of the contact

A commonly recurring question when working with organic devices is the effect of the chosen metal contact on the performance of the device. Most contacts induce an injection barrier[34] to the organic layer because of the difficulty in achieving Ohmic contacts. Different contact materials will change the carrier injection and as such the characteristics of the device. Stössel *et al.*[35] evaluated the performance of organic light-emitting diodes (OLEDs) by using a range of cathodes with different work functions. Their results revealed a clear relationship between efficiency of the OLED and cathode metal work function. Although the effective injection barrier is not known, the injection barrier will scale with the work function of the metal, which is measured or calculated for a clean surface.[23,36] For some small molecules, such as C_{60}, the interaction between organic and the metal contact is large enough that the injection barrier is pinned to a certain value, regardless of which metal is used.[37] To avoid these problems, PTCDI-$C_{13}H_{27}$ is used as an acceptor material as it is known that for this acceptor, different contact metals change the injection behavior.[38] For the comparison to the model, we modify the injection barrier at the donor side, but *mutatis mutandis*, this is equivalent to the experimental situation of modifying the barrier at the acceptor side.

The results of a simulation with different injection barriers at the donor side can be seen in Fig. 5, where the resistance at V_{oc} is plotted versus the carrier density at the interface for a 50 nm thick layer. With increasing injection barrier, the carrier density at the contact drops [see Eq. (8)]. As can be seen in Fig. 2, a decreasing carrier density at the contact will change the steady state carrier density throughout the layer. As expected from Eq. (22), the resistance drops with increasing carrier density at the interface until the point where the increase has only an effect on the carrier profile close to the interface. The lower carrier density elsewhere in the layer will dominate and the resistance will remain constant. The point where the resistance exponentially stops decreasing is shifted depending on the metal work function. Higher injection barriers shift this point to lower light intensities and, consequently, the saturated resistance is higher.

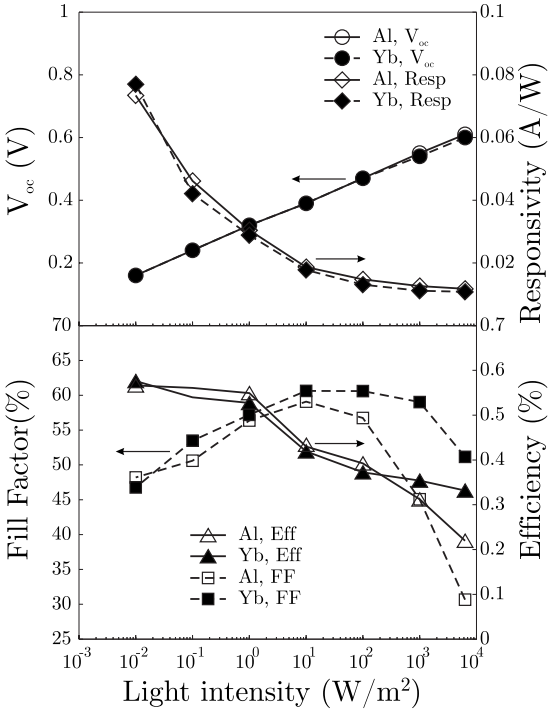

FIG. 6. Extracted light dependent parameters from planar heterojunction solar cells, consisting of 50 nm CuPc, 50 nm PTCDI-$C_{13}H_{27}$, and a metal contact. The top contact is Yb or Al.

Experimentally, two different metals [ytterbium (Yb) and aluminum (Al), with reported work functions of 2.63 and 4.30 eV, respectively[23,35]] are deposited as cathode on a planar heterojunction composed of 50 nm CuPc followed by 50 nm PTCDI-$C_{13}H_{27}$. The resulting parameters of the light-dependent *I-V* measurements are displayed in Fig. 6. For both cells, the responsivity, which is the short-circuit (I_{sc}) current divided by the incident light power (P_0), decreases with increasing P_0.

V_{oc} logarithmically increases with illumination intensity, with a slope of 75 mV/decade. This is not equal to the expected value (60 or 120 mV) due to the decreasing responsivity, as shown in Fig. 6. The decreasing responsivity reflects a decreasing free carrier generation efficiency at the interface, corresponding to κ (or the different recombination terms) in Eq. (19) being dependent on the light intensity. To take this into account, we fit the responsivity as a function of P_0 by using a power law (responsivity $\propto P_0^{2/3}$ or $\kappa \propto P_0^{2/3}$). The apparent slope of 75 mV/decade corresponds to $3/2\times75$ mV/decade=113 mV/decade. This is very close to 120 mV, expected for SRH-type recombination. We conclude that SRH-type recombination is operative over 6 orders of magnitude in light intensity.

Within the measurement accuracy (10 mV), the two V_{oc} curves are identical for the different metals. V_{oc} does not change, although the forward current in the dark does. This proves the independence of V_{oc} with changing work function, as predicted by the model.

The dark *I-V* curves are fitted to the generalized Shockley equation,[39]

TABLE I. Parameters from dark IV-curves fitted with the generalized Shockley equation for the different samples

Sample	J_S (A/m^2)	n	R_s (Ω m^2)	R_p (Ω m^2)
Work function experiments (50 nm PTCDI-$C_{13}H_{27}$)				
Yb cathode	1.0×10^{-5}	1.6	11×10^{-4}	1.7×10^{5}
Al cathode	2.1×10^{-5}	1.7	11×10^{-3}	4.7×10^{5}
Thickness experiments (BCP/Al cathode)				
76 nm PTCDI-$C_{13}H_{27}$	1.7×10^{-4}	1.8	1.3×10^{-4}	2.6×10^{2}
152 nm PTCDI-$C_{13}H_{27}$	1.2×10^{-4}	1.8	5.5×10^{-4}	2.3×10^{2}
228 nm PTCDI-$C_{13}H_{27}$	1.4×10^{-4}	1.7	25.0×10^{-4}	0.8×10^{2}

$$I=\frac{R_p}{R_s+R_p}\left\{J_S\left[\exp\left(\frac{q(V-JR_s)}{nkT}\right)-1\right]+\frac{V}{R_p}\right\}, \quad (23)$$

where n is the diode ideality factor, J_S is the reverse saturation current, and R_s and R_p are the series and parallel resistances, respectively. The extracted fit parameters (Table I) are comparable for both solar cells, with the exception of R_s. At high voltages or high P_0, R_s dominates. In that sense, R_s is a good value for R_{Voc} for high P_0, provided that R_s is independent of the incident light intensity P_0.

The resistance at V_{oc} vs P_0 is plotted in Fig. 7. The trends of the simulated data (Fig. 5) are apparent. The resistance exponentially decreases until it saturates toward the series resistance. The fill factor follows this trend: lower FF for the case with Al are visible at high light intensities. A more detailed look at the effects of resistance on FF can be found elsewhere in the literature.[18]

C. Thickness dependence

As mentioned in Sec. II D, a second parameter that influences R_{Voc} is the thickness of the organic layers. Simulations show two different regimes, depending on the boundary carrier concentrations at the contact and at the interface. If both are low, R_{Voc} will linearly increase with increasing thickness because the change in carrier density profile is negligible in comparison to the change in thickness. However, if the boundary concentrations are high, a third-order power-law dependence on the thickness will be visible. Figure 8 shows the reason of this power law. The carrier density forms a U shape, where the minimum carrier density is situated in the middle of the layer, and not at the boundaries. For thicker layers, the minimum carrier density is smaller. This effect adds up to the normal increase in resistance due to a longer travel distance.

The layer structure used in the experiments is 20 nm CuPc, followed by PTCDI-$C_{13}H_{27}$ to form the donor-acceptor interface, which is capped with 10 nm BCP and 80 nm Al to form the cathode. The layer thickness of PTCDI-$C_{13}H_{27}$ is varied from 78 to 228 nm. The dark I-V curves are seen in Fig. 9. The fitted parameters from Eq. (23) can be found in Table I. As seen before, R_{Voc} as a function of the incident light intensity has an asymptote toward the series resistance. The inset of Fig. 9 plots the series resistance versus the thickness. The trend is clearly superlinear.

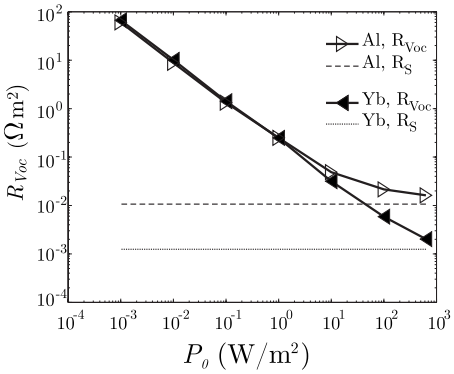

FIG. 7. The measured resistance at V_{oc} versus incident light power (P_0) for planar solar cells with Yb and Al as contact. As a guide for the eye, the dotted and the dashed lines represent the fitted dark series resistance R_S for cells with Al and Yb respectively.

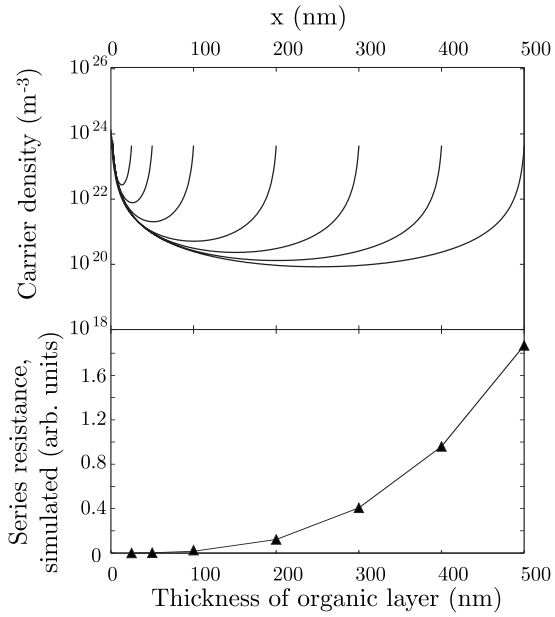

FIG. 8. Upper panel: calculated carrier profile inside layers with different thickness, from 25 nm to 500 nm, and with a mobility of 1×10^{-7} m^2/V s. The carrier density at the contact and the interface is kept constant at 1×10^{24} carriers/m^3. Lower panel: the resulting resistance at V_{oc} for the different thicknesses.

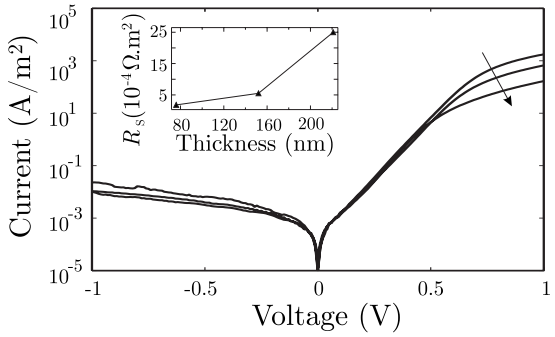

FIG. 9. The dark *I-V* curves for the solar cells with different PTCDI-$C_{13}H_{27}$ thicknesses and the arrow points to thicker PTCDI-$C_{13}H_{27}$ layers. Inset: series resistance dependence on thickness.

As a side note, the resistance dependence at high light intensities is related to the classical space-charge limited current (SCLC). In the SCLC model, the current is limited by the bulk itself, and not by injection of carriers at the contact. In our case, one of the contacts of the classical space-charge limited current is replaced by the interface between donor and acceptor, and as a result, we observe the same thickness dependence.

V. CONCLUSIONS

Starting from basic continuity equations, we have presented an analytical model for the open-circuit voltage regime of planar heterojunction solar cells. This model indicates that V_{oc} does not depend on the work function of the metal contacts. When the work function creates a low injection barrier, drift current will induce V_{oc}. If a high injection barrier is created, diffusion current of carriers away from the interface will make sure that the same V_{oc} is reached. The exact relationship between V_{oc} and P_0 is determined by the actual recombination process of free carriers at the interface.

An extension of the model focuses on the resistance of the solar cell at V_{oc}. This resistance is determined by the carrier profile inside the organic layers; the higher the carrier density, the lower the resistance. The carrier profile at zero current is determined by the boundary values, namely, the carrier density at the interface and at the contact. In this view, a change in the work function of the contact metal, leading to a change in carrier density at the contact, will affect the resistance, and hence, the FF. The lowest resistance will be reached when the carrier density is high or when the injection barrier is low. Metals with work functions close to the HOMO of the donor material or the LUMO of the acceptor material will lead to low resistive organic solar cells.

The effect of the thickness on the resistance is twofold. Thicker layers will lead to a longer distance the carriers need to travel. A second effect is the change in steady-state carrier densities. The minimum carrier density in the layer will be reduced when increasing the thickness. This point of lowest carrier density is the point of highest resistivity, and any change in this density will be reflected in the overall resistance of the layer. At high light intensities, these two effects add up and the resistance follows a third-order power law of the incident light intensity.

The results of these simulations can be applied to optimize organic planar heterojunction solar cells. For example, novel promising organic materials sometimes result in high resistive solar cells. Often, this high resistance is explained by a low mobility of the material; however, a better choice of contacts along with an optimized layer thickness could also reduce the resistance.

ACKNOWLEDGMENTS

The authors thank Vladimir Arkhipov for his fruitful discussions and lectures. This work was supported by the EU Integrated Project NAIMO (Grant No. NMP4-CT-2004-500355).

APPENDIX A: SOLUTION OF DIFFERENTIAL EQUATION FOR $p(x)$ AND $F(x)$

By using the Poisson equation [Eq. (2)] for holes only with zero net current ($j_p=0$), Eq. (6) can be reformulated as

$$F\frac{dF}{dx} - \frac{kT}{q}\frac{d^2F}{dx^2} = 0. \tag{A1}$$

A double substitution ($x=-u2kT/q$ and $F=y'/y$) is carried out, yielding the following differential equation:

$$y'' = C_1 y. \tag{A2}$$

The differential equation can be solved depending on the value of the integration constant C_1. This latter parameter is determined by the boundary conditions: the electric field (F_c) and the carrier density (p_c) at the contact,

$$C_1 = F_c^2 - \frac{2kT}{\varepsilon}p_c. \tag{A3}$$

Case 1: $C_1<0$. The solution can be expressed as

$$y = A\cos(\pm\sqrt{-C_1}u + C_2), \tag{A4}$$

where A and C_2 are the two more integration constants. As F is equal to y'/y, the integration constant A disappears. The field and the carrier density can be rewritten as

$$F(x) = \mp\sqrt{-C_1}\tan\left(\mp\sqrt{-C_1}\frac{q}{2kT}x + C_2\right), \tag{A5}$$

$$p(x) = \frac{\varepsilon}{2kT}\frac{-C_1}{\cos^2\left(\mp\sqrt{-C_1}\frac{q}{2kT}x + C_2\right)}, \tag{A6}$$

with the integration parameter C_2 that can be expressed in terms of F_c and p_c,

$$C_2 = \arctan\left(\mp\frac{1}{\sqrt{\frac{2kT}{\varepsilon}\frac{p_c}{F_c^2} - 1}}\right). \tag{A7}$$

Case 2: $C_1=0$. This case can be seen as a boundary case. The solution is

$$y = A(u + C_2). \tag{A8}$$

The field and the carrier density can be written as

$$F(x) = \frac{-1}{\frac{q}{2kT}x - C_2}, \tag{A9}$$

$$p(x) = \frac{\varepsilon}{2kT} \cdot \frac{1}{\left(\frac{q}{2kT}x - C_2\right)^2}, \tag{A10}$$

with

$$C_2 = \frac{1}{F_c}. \tag{A11}$$

Case 3: $C_1 > 0$. Two solutions are possible,

$$y = A \sinh(\pm\sqrt{C_1}u + C_2), \tag{A12}$$

or

$$y = A \cosh(\pm\sqrt{C_1}u + C_2), \tag{A13}$$

but the solution with the cosh is nonphysical as it leads to negative charge densities. Again, equations for field and carrier density can be calculated as

$$F(x) = \pm\sqrt{C_1}\coth\left(\mp\sqrt{C_1}\frac{q}{2kT}x + C_2\right), \tag{A14}$$

$$p(x) = \frac{\varepsilon}{2kT}\frac{C_1}{\sinh^2\left(\mp\sqrt{C_1}\frac{q}{2kT}x + C_2\right)}, \tag{A15}$$

with

$$C_2 = \sec\left(\pm\frac{1}{\sqrt{1 - \frac{2kT}{\varepsilon}\frac{p_c}{F_c^2}}}\right). \tag{A16}$$

APPENDIX B: SOLUTION OF INTEGRAL EQUATION FOR R_{voc}

The sign of the integration constant C_1 [Eq. (A3)] will determine the solution of Eq. (22). To simplify the equations, two parameters (β and γ) are defined as

$$\beta = 1 - \frac{C_1}{F_c^2}, \tag{B1}$$

$$\gamma = 2d_D\frac{\sqrt{C_1}}{kT/q}. \tag{B2}$$

The solutions of the integral are as follows:
For $C_1 > 0$ or $\beta < 1$,

$$R_{\text{voc}} = \frac{d_D^3}{\varepsilon\mu_p kT/q} \times \frac{\{\sinh\gamma[(2-\beta)\cosh\gamma - 2\sqrt{1-\beta}\sinh\gamma] - \gamma\beta\}}{\gamma^3\beta}. \tag{B3}$$

For $C_1 < 0$ or $\beta > 1$,

$$R_{\text{voc}} = \frac{d_D^3}{\varepsilon\mu_p kT/q}\frac{\{\sin\gamma[(\beta-2)\cos\gamma - 2\sqrt{\beta-1}\sin\gamma] - \gamma\beta\}}{\gamma^3\beta}. \tag{B4}$$

*david.cheyns@imec.be
†Present address: Experimental Physics VI, Julius-Maximilians-University of Würzburg, Am Hubland, 97074 Würzburg, Germany.

[1] C. W. Tang, Appl. Phys. Lett. **48**, 183 (1986).
[2] P. Peumans and S. R. Forrest, Appl. Phys. Lett. **79**, 126 (2001).
[3] W. Geens, T. Aernouts, J. Poortmans, and G. Hadziioannou, Thin Solid Films **403-404**, 438 (2002).
[4] S. Yoo, B. Domercq, and B. Kippelen, Appl. Phys. Lett. **85**, 5427 (2004).
[5] B. Maennig *et al.*, Appl. Phys. A: Mater. Sci. Process. **79**, 1 (2004).
[6] C. W. Chu, Y. Shao, V. Shrotriya, and Y. Yang, Appl. Phys. Lett. **86**, 243506 (2005).
[7] B. P. Rand, J. Xue, F. Yang, and S. R. Forrest, Appl. Phys. Lett. **87**, 233508 (2005).
[8] P. Liu, Q. Li, M. Huang, W. Pan, and W. Deng, Appl. Phys. Lett. **89**, 213501 (2006).
[9] K. L. Mutolo, E. I. Mayo, B. P. Rand, S. R. Forrest, and M. E. Thompson, J. Am. Chem. Soc. **128**, 8108 (2006).
[10] D. Cheyns, H. Gommans, M. Odijk, J. Poortmans, and P. Heremans, Sol. Energy Mater. Sol. Cells **91**, 399 (2007).
[11] B. Mazhari, Sol. Energy Mater. Sol. Cells **90**, 1021 (2006).
[12] M. C. Scharber, D. Mühlbacher, M. Koppe, P. Denk, C. Waldauf, A. J. Heeger, and C. J. Brabec, Adv. Mater. (Weinheim, Ger.) **18**, 789 (2006).
[13] J. A. Barker, C. M. Ramsdale, and N. C. Greenham, Phys. Rev. B **67**, 075205 (2003).
[14] M. Koehler, L. S. Roman, O. Inganäs, and M. G. E. da Luz, J. Appl. Phys. **96**, 40 (2004).
[15] A. Gadisa, M. Svensson, M. R. Andersson, and O. Inganäs, Appl. Phys. Lett. **84**, 1609 (2004).
[16] B. P. Rand, D. P. Burk, and S. R. Forrest, Phys. Rev. B **75**, 115327 (2007).
[17] J. Xue, S. Uchida, B. P. Rand, and S. R. Forrest, Appl. Phys. Lett. **84**, 3013 (2004).
[18] S. Yoo, B. Domercq, and B. Kippelen, J. Appl. Phys. **97**, 103706 (2005).
[19] J. C. Scott, J. Vac. Sci. Technol. A **21**, 521 (2003).
[20] V. I. Arkhipov, in *Conjugated Polymer and Molecular Interfaces*, edited by W. R. Salaneck, K. Seki, A. Kahn, and J. Pireaux (Dekker, New York, 2002), Chap. 19, pp. 613–650.
[21] H. Ishii, K. Sugiyama, E. Ito, and K. Seki, Adv. Mater. (Weinheim, Ger.) **11**, 605 (1999).
[22] A. Wan, J. Hwang, F. Amy, and A. Kahn, Org. Electron. **6**, 47 (2005).

[23] S. M. Zse, *Physics of Semiconductor Devices* (Wiley, New York, 1981).
[24] B. A. Gregg and M. C. Hanna, J. Appl. Phys. **93**, 3605 (2003).
[25] L. A. A. Pettersson, L. S. Roman, and O. Inganäs, J. Appl. Phys. **86**, 487 (1999).
[26] R. M. A. Azzam and N. M. Bashara, *Ellipsometry and Polarized Light* (Elsevier, New York, 1987).
[27] C. L. Braun, J. Chem. Phys. **80**, 4157 (1984).
[28] A. C. Morteani, P. Sreearunothai, L. M. Herz, R. H. Friend, and C. Silva, Phys. Rev. Lett. **92**, 247402 (2004).
[29] M. Mandoc, W. Veurman, and L. Koster, B. deBoer, and P. Blom, Adv. Funct. Mater. **17**, 2167 (2007).
[30] W. Shockley and W. T. Read, Phys. Rev. **87**, 835 (1952).
[31] R. N. Hall, Phys. Rev. **87**, 387 (1952).
[32] M. M. Mandoc, F. B. Kooistra, J. C. Hummelen, B. de Boer, and P. W. M. Blom, Appl. Phys. Lett. **91**, 263505 (2007).
[33] V. Shrotriya, G. Li, Y. Yao, T. Moriarty, K. Emery, and Y. Yang, Adv. Funct. Mater. **16**, 2016 (2006).
[34] T. P. Nguyen and P. Destruel, in *Handbook of Luminescence, Display Materials, and Devices*, edited by H. S. Nalwa and L. S. Rohwer (American Scientific, Stevenson Ranch, CA, 2003), Vol. 1, Chap. 1, pp. 1–130.
[35] M. Stössel, J. Staudigel, F. Steuber, J. Simmerer, and A. Winnacker, Appl. Phys. A: Mater. Sci. Process. **68**, 387 (1999).
[36] D. R. Lide, *Handbook of Chemistry and Physics*, 85th ed. (CRC, New York, 2003).
[37] C. J. Brabec, A. Cravino, D. Meissner, N. S. Sariciftci, T. Fromherz, M. T. Rispens, L. Sanchez, and J. C. Hummelen, Adv. Funct. Mater. **11**, 374 (2001).
[38] D. J. Gundlach, K. P. Pernstich, G. Wilckens, M. Gruter, S. Haas, and B. Batlogg, J. Appl. Phys. **98**, 064502 (2005).
[39] R. H. Bube and A. L. Fahrenbruch, *Advances in Electronics and Electron Physics* (Academic, New York, 1981).